International Journal of Mechanical, Industrial and Aerospace Sciences
ISSN: 2517-9950
Vol:6, No:5, 2012

Investigation of behavior on the Contact Surface of the Tire and Ground by CFD Simulation

M. F. Sung, Y.D. Kuan*, R.J. Shyu, S.M. Lee.

***Abstract*—**Tread design has evolved over the years to achieve the common tread pattern used in current vehicles. However, to meet safety and comfort requirements, tread design considers more than one design factor. Tread design must consider the grip and drainage, and the manner in which to reduce rolling noise, which is one of the main factors considered by manufacturers. The main objective of this study was the application the computational fluid dynamics (CFD) technique to simulate the contact surface of the tire and ground. The results demonstrated an air-Pumping and large pressure drop effect in the process of contact surface. The results also revealed that the pressure can be used to analyze sound pressure level (SPL).

***Keyword*—**Air-pumping, computational fluid dynamics, sound pressure level, tire.

I. Introduction

THE first car was manufactured on January 29, 1886. Cars were widely available because of the advances in technology and production. Most of the street noise originated from the cars. Therefore, identification of the sources and reduction of car noise has become a crucial goal in recent years. Technological progress has enabled considerable improvements of several crucial sources of noise, such as running engines, intake and exhaust noise, cooling fan noise, transmission system, and car shells affected by wind noise. The tire noise generated by rolling of the tires has been confirmed as one of the sources of noise [1], [2]. Consequently, the Economic Commission for Europe (ECE) developed a new standard called ECE-R117 [3] in 2009. It requires that tires must comply with objectives within a specific period, such as fuel efficiency, wet grip performance, rolling resistance, and noise level. Therefore, this study discussed the relationship between contact surface of the tire and ground. For a specific area to produce a greater pressure drop, noise may be generated by geometric change to reduce the pressure, which reduces the noise level. Kim et al. [4] applied a simplified model to investigate the effect of tire air-pumping and the intensity of the noise. The model can be built on a simple 2D tread pattern with two plates (direction-X and direction-Y) to simulate the squeezing of a tire groove as it enters the contact patch between the tire groove and the road surface.

M. F. Sung, is a postdoctoral researcher with Department of Refrigeration, Air Conditioning and Energy Engineering, National Chin-Yi University of Technology, Taiwan, (e-mail: song221@gmail.com).

Y. D. Kuan*, is a professor with Department of Refrigeration, Air Conditioning and Energy Engineering, National Chin-Yi University of Technology, Taiwan, (phone: 886-4-23924505 ext8256; fax: 886-4-23923380; e-mail: ydkuan@ncut.edu.tw).

R. J. Shyu, is a professor with Department of Systems Engineering and Naval Architecture, National Taiwan Ocean University, Taiwan, (e-mail: rjs@mail.ntou.edu.tw).

S. M. Lee, is a associate professor with Department of Aerospace Engineering, Tamkang University, Taiwan,(e-mail: 061503@mail.tku.edu.tw).

The proposed method can be divided into three steps, as follows: small-scale noise generation simulation; noise propagation simulation; and far-field acoustic pressure prediction. Based on the results, when the tire groove ground and released from the contact patch, the tread generated the compressed effect, which caused a large pressure drop and generated noise. Eisenblaetter et al. [5] proposed that the main objective of the rolling noise is air-pumping, followed by air resonant radiation and pipe resonances. In addition, similar to tire noise analysis methods, such as the application of FEM, this method had an important point to be considered as coincidence between the structural and cavity modes.[6], [7]. Bueno et al. [8] proposed that pavement temperature can also influence tire and road noise. Their experimental results demonstrated that temperature leads to a reduction in the close proximity sound levels assessed at a rate of 0.06 dB(A)/℃. These results were used to discuss the proposed methods of tire noise, which are helpful in reducing the generated noise

II. Numerical Simulation

A. Model Structure

The schematic for contact surface of the tire and ground is shown in Fig. 1. Figure 1(a) shows rolling tires. Figure 1(b) shows the tire groove at a 45° angle with the ground, because the tire groove began to compress and reduce the gap because of air-pumping effect. Figure 1(c) shows the tire groove at a 90° angle with the ground; the groove compression increased the internal pressure. Figure 1(d) shows the tire groove at a 135° angle with the ground, and the instant gap caused an instant release of pressure of the tire grooves, which affects the air-pumping. As shown in Figure 1(e), when the tire continued rolling, the groove recovery allowed the default pressure-direction to change to the negative direction. Consequently, the contact surface of the tire and ground can be designed based on this phenomenon, as shown in the simplified model in Fig. 2. This simplified model is made by the T type rectangle, and the boundary was set as follows: free outlet, wall, deform, plate_x, and plate_y. The Y direction of plate_y moves up and down by the timetable, which simulates the tire groove compression. The X direction of plate_x moves to another side to simulate the contact surface of the tire rolling process. The X direction of plate_x moves according to the conversion by Equation (1) and (2). In Equation (1), the unit of (a) is the simulation car speed (km/hr); therefore, it must be exchanged to (b) (m/s). Finally, tire groove pitch is divided (c) by the speed (a), such as 1.2, to determine the total simulation time scale. This indicates that the X direction of the plate_x starts moving parallel and must finish at this time scale. The dimensions and numerical settings are listed in Table I.

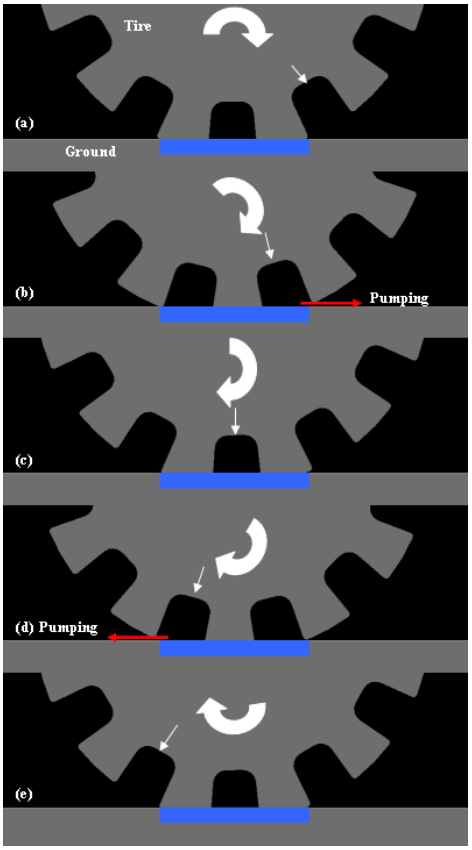

Fig. 1 The schematic for contact surface of the tire and ground

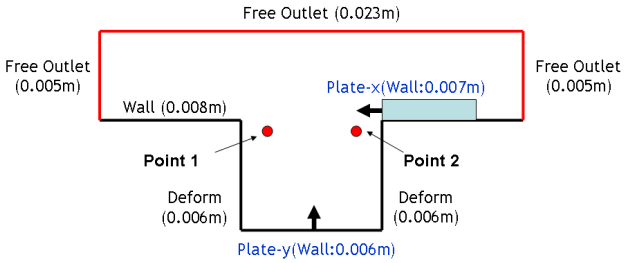

Fig. 2 The simplified model for contact surface of the tire and ground

$$a_{speed} = \frac{b_{speed} \times 1000}{3600} \quad (1)$$

$$d_{sec} = \frac{c_{pitch}}{a_{speed}} \quad (2)$$

TABLE I
THE DIMENSIONS AND NUMERICAL SETTINGS

Notation	Physical quantity	Dimension	Value
a	car speed(converter)	m/s	27.8
b	car speed(default)	km/h	100
c	adjustment of the tread pitch	M	0.0556
d	simulation time	s	0.002
plate_x	moving body plate-x	m	0.007
plate_y	moving body plate-y	m	0.006
Deform	deform plane	m	0.006
T	reference temperature	°K	273

In addition, to simulate various loads or rubber materials, the Y direction of plate movement was set to three different types of compression speeds, that is, 1, 2, and 4 m/s. Its operation time is shown in Fig. 3. After several simulations, the X direction of plate_x moving speed condition set at -7m/s was completed in a total simulation time scale of 0.02 s. In the Y direction, parts of at the plate_y setup 1, -1, 2, -2, 4, -4 three speed case. In case 1, when simulation time from zero to 0.001 s, the Y direction of plate_y changed the moving speed from 1 to -1. The Y direction of the plate moving speed changed from 2 to -2 for case 2, In which the tire groove compression was simulated. To further observe the compression pressure in the contact surface of the tire and ground, this study set the tire at the two monitoring points, the locations of which were named point 1 (set point at -0.2, -0.05) and point 2 (set point at 0.2, -0.05).

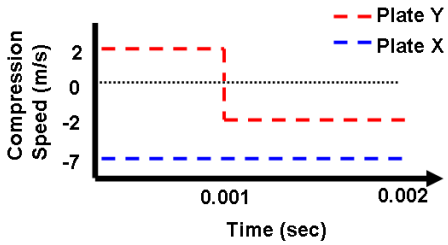

Fig. 3 The X and Y directions of the plate operation time

B. Simulation model define

1. Mesh

This study used the Capvidia developed commercial fluid dynamics software, FlowVision, for simulation and analysis. This software was used by the grid establishment of technology (Sub Grid Geometry Resolution, SGGR) against complex objects, such as contact surface of the tire and ground, as shown in Fig. 4. In this study, the simulation model was established by the grid number for 7020. To enhance the solving accuracy, this study also enabled the split technique of the software to enhance the accuracy of moving objects, such as X direction of the plate. Based on this technique available automatically complete during the simulation, as shown in Fig. 5, which demonstrates remeshing in any time, and the original grid is retained, not due the plate move and deformation. This approach can reduce the simulation time and enhance the solving accuracy.

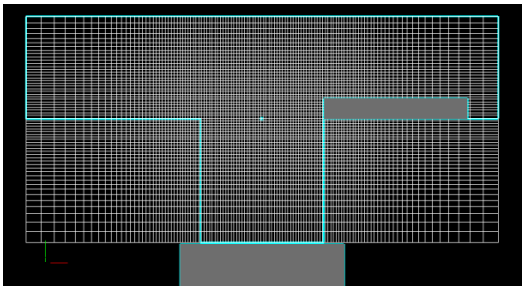

Fig. 4 The grid establishment of technology (SGGR)

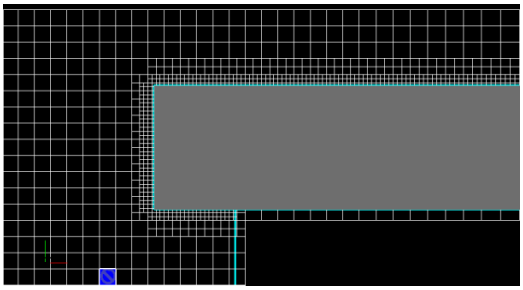
Fig. 5 Automatically remeshing for plate_x

2. Simulation Theory

Several types of numerical methods are used, the most common of which include finite element method (FE), finite difference method (FD), and finite volume method (FV). In this study, the CFD software used the finite volume method. Because the finite element method has a fast solution speed, it has been widely applied in timeliness and correctness of various application areas, such as automobiles, aviation, shipping, and industry, to solve the deformation problems. Equation (3) is the basis of the formula of the finite volume method, where Ω is cell volume; and ΔS_i is area of the i - the cell face.

$$\int_{\Omega} (\nabla \cdot F) d\Omega = \sum_{i-faces} (F_i \cdot n_i) \cdot \Delta S_i \tag{3}$$

However, the main objective of the study was to investigate behavior of the tire and ground on the contact surface; therefore, the simulated fluid was gas, without consideration of heat transfer. The units and numerical settings are listed in Table II. Equation (4) was used to solve the total pressure, where R_A is universal gas constant; the default was 8.31441. By balancing Equation (4), it can be rewritten as Equation (5), as follows:

$$P_{tot} = P_{abs}\left(\frac{T_{tot} + T_{ref}}{T_{abs}}\right)^{\frac{C_p}{R_A/m}} - P_{ref} \tag{4}$$

$$P_{abs} = \frac{\rho R_A T_{abs}}{m} \tag{5}$$

Equation (6) and (7) were used to solve the continuity equation and momentum equation. Because this study simulated the air flow field, it used the gas energy equation, (8).

TABLE II
THE UNITS AND NUMERICAL SETTINGS

Notation	Physical quantity	Dimension
C_p	specific heat	$m^2s^{-2}K^{-1}$
F	acceleration of external volume face	ms^{-2}
g	gravity acceleration	ms^{-2}
H	total enthalpy	m^2s^{-2}
k	turbulent energy	m^2s^{-2}
L	characteristic length	m
m	molar mass	$kgmile^{-1}$
P	relative pressure	Pa
P_{ref}	reference pressure	Pa
P_{hst}	hydrostatic pressure	Pa
P_{abs}	absolute pressure	Pa
P_{tot}	total pressure	Pa
Pr_t	turbulent prandtl number	----
P^n	pressure value at time layer n	Pa
P^{n+1}	pressure value at time layer n+1	Pa
Q	sum of the energy of different nature	m^2s^{-2}
R_A	universal gas constant	$Jmole^{-1}K^{-1}$
T_{tot}	total temperature	°K
T_{ref}	reference temperature = 273	°K
T_{abs}	absolute temperature	°K
T^n	temperature value at time layer n	°K
μ	molecular dynamic viscosity	$kgm^{-1}s^{-1}$
μ_t	turbulent dynamic viscosity	$kgm^{-1}s^{-1}$
V	relative velocity	m/s
V^n	velocity value at time layer n	m/s
ρ^n	density value at time layer n	$kg\ m^{-3}$
ρ^{n+1}	density value at time layer n+1	$kg\ m^{-3}$
ε	dissipation rate of turbulent energy	m^2s^{-2}
β	coefficient of thermal expansion	$°K^{-1}$
∂T	relative local specific	Kgs^{-2}

Because the turbulent model was considered, this study used Equation (9) and (10).

$$\frac{\partial_p}{\partial_t} + \nabla \cdot (\rho V) = 0 \tag{6}$$

$$\frac{\partial_p V}{\partial_t} + \nabla \cdot (\rho V \otimes V) = -\nabla P + \nabla \cdot \hat{\tau}_{eff} + \rho F \tag{7}$$

In here, $\hat{\tau}_{eff}$ is effective shear stress tensor.

$$\frac{\partial(\rho H)}{\partial t} + \nabla \cdot (\rho V H) = \frac{\partial P}{\partial t} + \nabla\left(\left(\frac{\lambda}{C_p} + \frac{\mu_t}{\mathrm{Pr}_t}\right)\nabla H\right) + \rho V \cdot F + Q \tag{8}$$

$$\frac{\partial(\rho k)}{\partial t} + \nabla \cdot (\rho V k) = \nabla\left(\left(\mu + \frac{\mu_t}{\sigma_k}\right)\nabla k\right) + \mu_t\left(G + \frac{\beta}{\mathrm{Pr}_t} g \cdot \nabla T\right) - \rho\varepsilon \tag{9}$$

$$\frac{\partial(\rho \varepsilon)}{\partial t} + \nabla \cdot (\rho V \varepsilon) = \nabla\left(\left(\mu + \frac{\mu_t}{\sigma_\varepsilon}\right)\nabla \varepsilon\right) + C_1 \frac{\varepsilon}{k}\mu_t\left(G + \frac{\beta}{\mathrm{Pr}_t} g \cdot \nabla T\right) - C_2 \rho \frac{\varepsilon^2}{k} \tag{10}$$

The model parameters and the expression for generation term G can be rewritten to Equation (11), (12), and (13).

$$G = D_{ij}\frac{\partial V_i}{\partial_{xj}} \tag{11}$$

$$D_{ij} = S_{ij} - \frac{2}{3}\left(\nabla \cdot V + \frac{\rho k}{\mu_t}\right)\delta_{ij} \tag{12}$$

$$S_{ij} = \frac{\partial V_i}{\partial x_j} + \frac{\partial V_j}{\partial x_i} \tag{13}$$

In addition, because of the movement of the plate in the X direction and Y direction, this study considered the Euler-equation and Navier-Stoke equation, and ignored the viscous. Equations (6), (7), (8), and (9), can solve the pressure equation, such as Equation (14) at one time step. From Equation (14), $\tilde{\rho}^{n+1}$ is intermediate pressure field and that can be rewritten to Equation (15). In addition, because of consider the ideal-gas, that can rewrite to such as Equations (16), (17), and (18), in which P_{abs} can be solved by Equation (16) [9].

$$\frac{\tilde{\rho}^{n+1} - \rho^n}{\tau} + \nabla(\rho^{n+1}V^n) = \tau(\Delta P^{n+1} - \Delta P^n) \tag{14}$$

$$\tilde{\rho}^{n+1} = \rho^n + \frac{\partial \rho}{\partial P}(P^n, T^n)(P^{n+1} - P^n) \tag{15}$$

$$P_{abs} = P_{ref} + P = \rho\frac{R_A T_{abs}}{m} \tag{16}$$

$$\frac{\partial \rho}{\partial P} = \frac{m}{R_A T_{abs}} \tag{17}$$

$$\tilde{\rho}^{n+1} = \frac{m}{R_A T_{abs}^n}\tilde{\rho}^{n+1} + \frac{m}{R_A T_{abs}^n}P_{ref} \tag{18}$$

III. Simulation Result

C. Result for Pressure

Figs. 6-8 show the simulation results for compression speeds at 1, 2, and 4 m/s. The results show that the maximal pressure in the compression speed is 4m/s, and minimal pressure in the compression speed is 1m/s. These results indicate that the tread in contact with the ground and leaving the ground produces a large pressure drop.

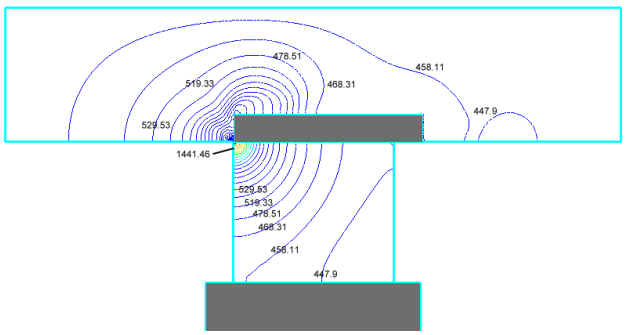

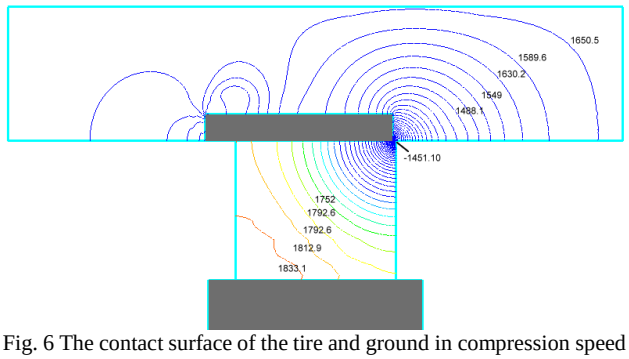

Fig. 6 The contact surface of the tire and ground in compression speed 1m/s

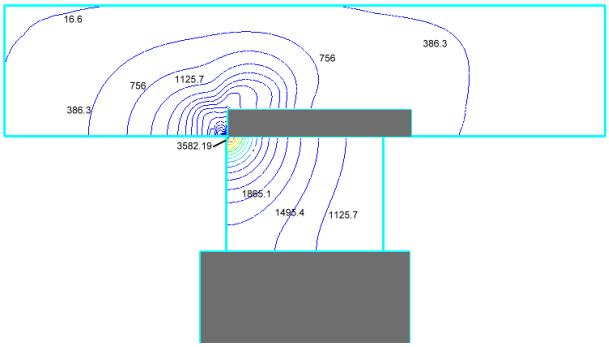

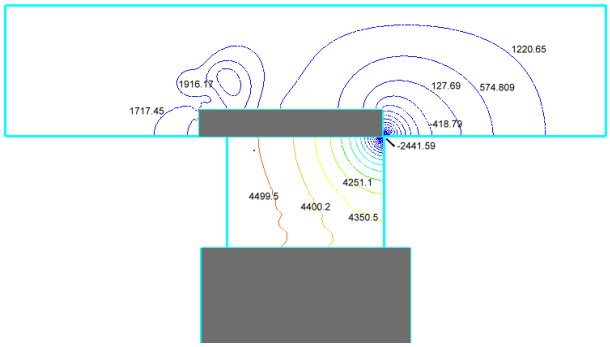

Fig. 7 The contact surface of the tire and ground in compression speed 2m/s

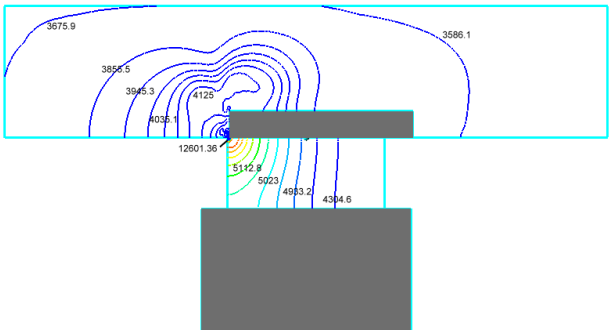

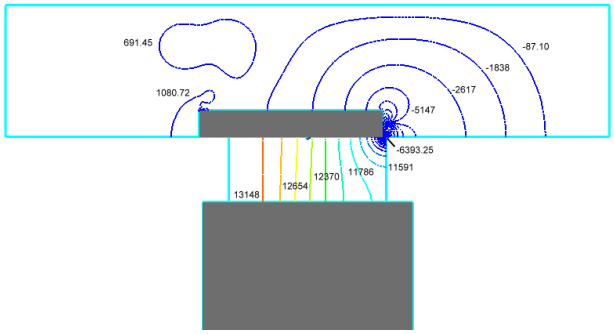

Fig. 8 The contact surface of the tire and ground in compression speed 4m/s

Fig. 9 and Table III show the pressure curve and value for the various compression speeds and simulation times. According to the results, the maximal pressure value at the compression speed of 4m/s was 12601.36 (Pa), and the minimal pressure value was -1451.10 (Pa). Therefore, the result demonstrates that large pressure drop occurs at contact surface of the tire and ground, and the direction of pressure is opposite. This indicates that the noise sources were generated at both time points (0.0009 s and 0.0011 s).

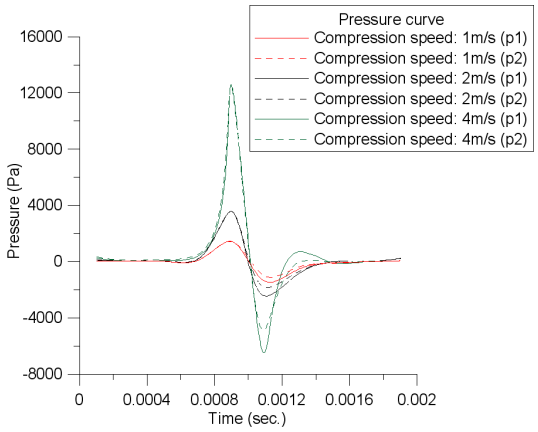

Fig. 9 The pressure curve for the compression speed and simulation time

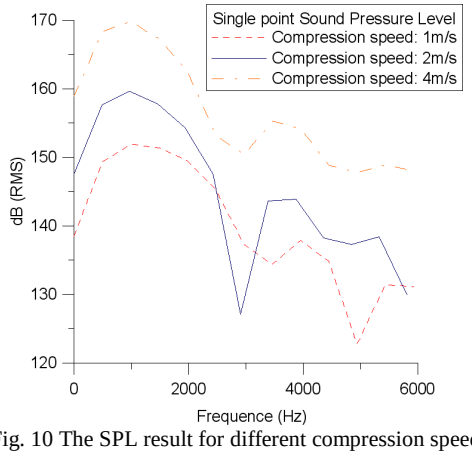

Fig. 10 The SPL result for different compression speed

TABLE III
THE MAXIMUM AND MINIMUM PRESSURE VALUE AT THE DIFFERENT COMPRESSION SPEED

Speed (m/s)	Max(Pa)	Min(Pa)
1	1441.46	-1451.10
2	3582.19	-2441.59
4	12601.36	-6393.25

Fig. 10 shows the single point sound pressure level (SPL) results for various compression speeds. The curve is the FFT converted from pressure; simulation time and sound pressure levels are also defined. The SPL can be written as Equation (19). The analysis was completed after FFT converted all of the data. The maximal SPL for compression speeds at 1, 2, and 4 m/s were 151.89 dB, 159.58 dB, and 169.81 dB, respectively. However, the SPL result shown only a single point at the simulation area, which decreases by transport, such as flow field velocity or temperature. Therefore, this SPL value was used to reference the trend for contact surface of the tire and ground noise.

$$SPL = L_p = 10\log_{10}\left(\frac{P_{rms}^{\ 2}}{P_{ref}^{\ 2}}\right) = 20\log_{10}\left(\frac{P_{rms}}{P_{ref}}\right) dB \qquad (19)$$

D.Result for Modify

A semicircular and rectangle design was used for the tire groove to reduce the pressure effect on contact surface of the tire and ground, as shown in Fig. 11. The simulation result demonstrated that, when the compression speed was 2 m/s, the first type design for semicircular generated maximal pressure value of 3228.14 (Pa), and the second type design for rectangle generated maximal pressure value of 2064.02 (Pa), as shown in Fig. 12.Compared to the original simulation results, the second type design for rectangle exhibited a decrease in the maximal pressure value of 27.16%.The maximal sound pressure level was 153.56 dB, as shown in Fig 13. Compared to the original simulation results, the rectangle type design exhibited a decrease in the sound pressure level value of 1.92%.

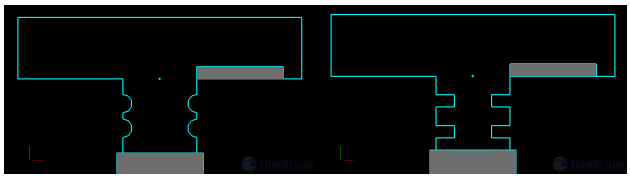
Fig. 11 Rectangle and semicircular design for tire groove

IV. Conclusion

The simulation results in this study demonstrated a considerable pressure drop generated by the contact surface process of the tire and ground. In addition, contact with the ground resulted in higher pressure than leaving the ground. The value of the difference is considerable, and exhibited different directionality. This can be used to analyze the noise, and design a suitable groove to reduce tire rolling noise. In addition a geometric design modification of the tire groove can effectively reduce the generated pressure, which can reduce tire rolling noise.

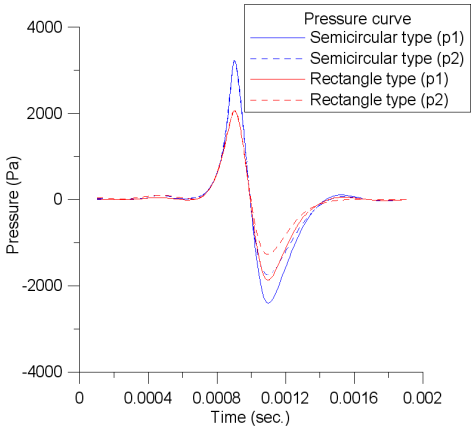

Fig. 12 The pressure curve for different design and simulation time at compression speed is 2 m/s

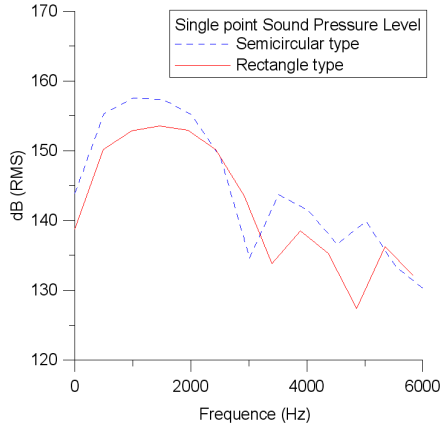

Fig. 13 The SPL result for Semicircular and Rectangle design at compression speed is 2 m/s

In noise analysis, this study also demonstrated that the maximal sound pressure level (SPL) for compression speed was 4 m/s. Finally, to reduce the SPL value, the second type design for rectangle generated maximal pressure and SPL reduction of 26.89% and 1.92%, respectively.

ACKNOWLEDGMENT

The author gratefully acknowledges the financial support provided to this study by the Ministry of Economic Affairs, Taiwan. No.100-EC-17-A-05-S1-168.

REFERENCE

[1] Anfosso-Le´de´e, Y. Pichaud, "Temperature effect on tyre–road noise," Applied Acoustics, Vol.68, 2007, pp.1-16.
[2] H. Bendtsen, "The Nordic prediction method for road traffic noise," The Science of the Total Environment, Vol.235, 1999, pp.331-338.
[3] http://www.unece.org/
[4] S. Kim, W. Jeong, Y. Park, S. Lee, "Prediction method for tire air-pumping noise using a hybrid technique," J. Acoust. Soc. Am, Vol.119, 2006, pp.3799-3812.
[5] J. Eisenblaetter, Stephen J. Walsh, Victor V. Krylov, "Air-related mechanisms of noise generation by solid rubber tyres with cavities," Applied Acoustics, Vol.71, 2010, pp.854–860.
[6] B. S. Kim, G. J. Kim, T. K. Lee, "The identification of sound generating mechanisms of tyres," Applied Acoustics , Vol.68, 2007, pp.114–133.
[7] M. Brinkmeier, U. Nackenhorst, S. Petersen, O. von Estorff, "A finite element approach for the simulation of tire rolling noise," J. of Sound and Vibration, Vol.309, 2008, pp.20–39.
[8] M. Bueno, J. Luong, U. Viñuela, F. Terán, S.E. Paje, "Pavement temperature influence on close proximity tire/road noise," Applied Acoustics , Vol.72, 2011, pp.829–835.
[9] FlowVision 3.08.01 User's Manual, Capvidia Inc., (2011)